PAPER

Synthesis and characterization of nanostructured MnO$_2$–CoO and its relevance as an opto-electronic humidity sensing device†

Samiksha Sikarwar,[a] B. C. Yadav, [ID] *[a] G. I. Dzhardimalieva, [ID] [b] N. D. Golubeva[b] and Pankaj Srivastava[a]

Metal carboxylates are widely used in science and technology and have been the subject of intense studies due to the practical importance of their products. The present paper reports the synthesis of MnO$_2$–CoO using metal carboxylates as precursors and the effect of humidity on the transmitted power through its thin film at room temperature. The refractive index of the material was found to be 1.445930 and the peak obtained from the photoluminescence spectra lies in the visible region. TEM reported a minimum grain size of ∼5.7 nm and SAED confirmed the crystalline nature of the material, which was further confirmed by XRD. Fluorescence characteristics also confirmed the low dimensionality of the material. The film was then investigated using SEM which exhibited the porous morphology. Through UV-Vis spectroscopy, it was found that the absorption of the film takes place in the UV region and the optical band-gap was observed to be 3.849 eV from the Tauc plot. The film was employed as a transmission based opto-electronic humidity sensor. Average sensitivity was found to be ∼2.225 μW/% RH with response and recovery times of 47 s and 59 s respectively. Experiments were repeated and the reproducibility of result was found to be ∼89%.

Introduction

Unique surface properties and high catalytic activity of metal oxides make them very attractive for various sensor applications.[1,2] Titanium, cerium, copper, iron, and manganese oxides have been widely used as catalysts, photocatalysts and electro-catalysts in a variety of reactions in organic synthesis.[3–6] Transition metal oxides, such as Mn$_2$O$_3$, Co$_3$O$_4$, NiO, *etc.*, are of interest for optical waveguide gas sensors.[7] V$_2$O$_5$ nanobelts (V$_2$O$_5$·xH$_2$O, V$_2$O$_5$·CTAB and V$_2$O$_5$ nanorods annealed at 400 °C) revealed the properties of an ethanol sensor with high selectivity and stability.[8] The Cu–CuO nanocomposite was successfully used to modify a glassy carbon electrode to detect H$_2$O$_2$ and glucose.[9]

Metal carboxylates are widely used in science and technology. They have been the subject of intense studies due to the practical importance of their products.[10] In particular, the controlled thermolysis of metal carboxylates can be considered as an effective way for the synthesis of nanocomposite

materials.[11] Owing to the formation of ferromagnetic Fe$_3$O$_4$ and CoFe$_2$O$_4$ nanoparticles, the thermolysis products of metal acrylates and their co-crystallizates behave as solid magnets with a coercive force of 0.18 T and the residual magnetization of 15.5 mT at room temperature.[12] The spinel ferrites Zn$_{0.5}$Mn$_{0.5}$Fe$_2$O$_4$,[13] CoFe$_2$O$_4$,[14] and MnFe$_2$O$_4$ [15] synthesized by pyrolysis of the corresponding polyacrylate salts exhibit superparamagnetic properties at room temperature.

Humidity measurement is one of the most required parameters for various applications not only for improving the quality of life but also for enhancing the industrial process.[16,17] Advancements in sensor manufacturing technologies lead the researchers to know the degree of efficiency with predictions based on simulation techniques and design aids to improve sensitivity and sensor quality along with time-saving.[18] The humidity plays very important role and has acquired such incredible significance due to the fact that these vapours consist of highly reactive dipolar molecules which get condensed on or evaporate from the surface even with small variations in temperature of the environment. Optical humidity sensors are better than their electronic counterparts due to their small size, low weight, immune towards electromagnetic disturbances, possibility of multiplexing information and working on high pressure and flammable environments.[19] Complex oxides containing cobalt and manganese show different oxidation states (Co^{2+}, Co^{3+}, Mn^{2+}, Mn^{3+}, and Mn^{4+})[20] and hence attractive distinct properties like enhanced tunable surface, specific

[a]Nanomaterials and Sensors Research Laboratory, Department of Physics, Babasaheb Bhimrao Ambedkar University, Lucknow-226025, U.P., India. E-mail: balchandra_yadav@rediffmail.com; Tel: +919450094590

[b]Laboratory of Metallopolymers, Institute of Problems of Chemical Physics, Russian Academy of Sciences, Chernogolovka, Moscow Region, 142432, Russia

† Electronic supplementary information (ESI) available. See DOI: 10.1039/c8ra01975d

desirable pseudocapacitance, energy density. Also they are easy to fabricate, have low cost, efficient structural properties, abundant in nature and environment friendly[21] and hence can be proved as an excellent material for humidity sensing. Also recently their multicomponent electrocatalysts have been fabricated, like Mn_3O_4–CoO/CNT, Co_3O_4/Co_2MnO_4 and graphene/CNT/Co_3O_4 which showed excellent performance towards ORR (Oxidation Reduction Reaction) catalysis.[22] A few works has been done on manganese oxide and cobalt oxide based humidity sensor. Kato *et al.* in 1997 investigated the sol–gel processed electrolytic manganese dioxide (EMD) as humidity sensor which showed good sensitivity between 50–80% RH.[23] In another work, K. Miyazaki *et al.* in the same year developed a potential-type humidity sensor based on M_1/MnO_x/M_2 galvanic cell system, where MnO_x is an EMD–clay mineral mixture, M_1 is Pt, and M_2 is Cu or Al. Clay mineral samples included kaolinite, bentonite, activated clay, zeolite, and muscovite. Silica sand was used as a reference material. The EMD–kaolinite mixture responded in a wider humidity region of 20–90% RH.[24] Similarly Yang *et al.* in 2011 studied a micro humidity sensor which consisted of interdigitated electrodes and cobalt oxide nanosheet sensing film (prepared by precipitation–oxidation method). The capacitance of the sensor changes with the adsorption/desorption of water vapor.[25] In another work, Yadav *et al.* in 2013 investigated the multilayered sensing films prepared by sol–gel spin coating process using cobalt oxide precursor annealed at 450 °C which showed linear behavior towards entire range of % RH with average sensitivity of 0.76 μW/% RH.[26]

Previously our group has worked on yttria stabilized zirconia system and its opto-electronic humidity sensing[27] but sensitivity was found lesser. As MnO_2–CoO is a hygroscopic material and synthesized first time in our laboratory at low dimension with high aspect ratio, therefore in order to improve the sensitivity, nanostructured MnO_2–CoO has been investigated as an opto-electronic humidity sensor.

Experimental

Synthesis

Reagents. Ethylhexanoic acid (95%), Belgium, ACROS; $Co(NO_3)_2 \cdot 6H_2O$ (98%) (PANREAC reagent), $Mn(NO_3)_2 \cdot 4H_2O$ (PANREAC reagent) are used as received. Metal hexanoates were synthesized by the extraction method in the two-phase system of metal nitrate solution-organic acid by the following reaction given in eqn (1):

$$(M^{n+})_{aqua} + CH_3(CH_2)_3CH(C_2H_5)COOH \rightarrow$$
$$M[CH_3(CH_2)_3CH(C_2H_5)COO]_n + nH^+ \ldots \quad (1)$$
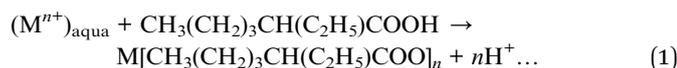
(M^{n+} – metal ion, n = 2, 3, 4).

For the synthesis of cobalt(II) ethylhexanoate, 45.5 g of cobalt(II) nitrate hydrate was dissolved in 160 ml of H_2O, and then the solution of metal nitrate was mixed with 80 ml of ethylhexanoic acid at pH 5 by adding NH_4OH. The resulting mixture was stirred for 1 h at room temperature, then after 12 h water phase was isolated in a separation funnel. For the

synthesis of manganese ethylhexanoate, 46.5 g of manganese(II) nitrate hydrate was dissolved in 400 ml of H_2O, then the solution of metal nitrate was mixed with 205 ml of ethylhexanoic acid at pH 5.6 by adding NH_4OH. The mixture was stirred for 1 h at room temperature, then after 12 h water phase was isolated in a separation funnel. The contents of cobalt and manganese in the extracts were 64 and 47.2 g kg^{-1}, respectively obtained after elemental analysis of the products on the atomic absorption spectrometer AAS-3. Then the mixture of metal hexanoate's extracts in the required ratio (1 : 2 by weight) was stirred for 20 min at 105–108 °C followed by vacuum distillation at 150 °C for 10 h. The Co : Mn : O atomic ratio in the product obtained was equal to 1.5 : 1.5 : 4 determined by quantitative chemical analysis.

Fabrication of sensing element

Porosity and regularity of the deposited film can be restricted by monitoring the sample preparation environment like gel density/viscosity, velocity of the spinner and heating/annealing temperature. Spin coating technique was used to deposit uniform sol–gel precursor MnO_2–CoO thin film with nanoscale on flat borosilicate substrates[28] having dimensions 1.5 × 1.5 cm^2 using a photoresist spinner (METREX RC100, India). Prior to spin coating, the flat borosilicate substrates were rinsed thoroughly with deionized water and isopropyl alcohol followed by acetone ultrasonically for 15 min each in order to remove microscopic contaminations.[29] The cleaned substrates were dried in an electric oven (METREX) at 100 °C for half an hour to remove the organic precursors and moisture completely from them. A small amount of gel was dropped on the centre of the substrate and then rotated at high speed in order to extend the gel by centrifugal force on the whole substrate. The rotation was sustained for 60 s at 3000 rpm so that fluid spins off the edges of the substrate and desired thickness of the film could be achieved.[30] After thin film formation, they were kept for drying on a hot plate at 60 °C for 15 min and then annealed at 650 °C for 3 h in a tubular electric furnace (METREX) in 78% nitrogen. Further, these films were used as sensing elements to investigate them as opto-electronic humidity sensing based on transmission.

Description of sensing set-up

The experimental set-up used for opto-electronic humidity sensing is shown in Fig. 1. It consists of 2 mW He–Ne LASER (Research Electro Optics Inc. 30 989) with 633 nm wavelength as input light source. A diverging lens of 10× magnification is used as beam expander for splitting the laser light beam so that it may incident and cover the whole surface of the sensing film. A glass chamber with humidity controlled system consisting of a hygrometer (HTC-1) of the range 10–90% RH along with a dish is kept inside for holding the humidifier/dehumidifier solution. The saturated solution of K_2SO_4/KOH (Fisher Scientific) in distilled water is used as humidifier/dehumidifier. The sensing element is fixed on one wall of the chamber such that it is perpendicular to the incident beam and also the beam covers the maximum
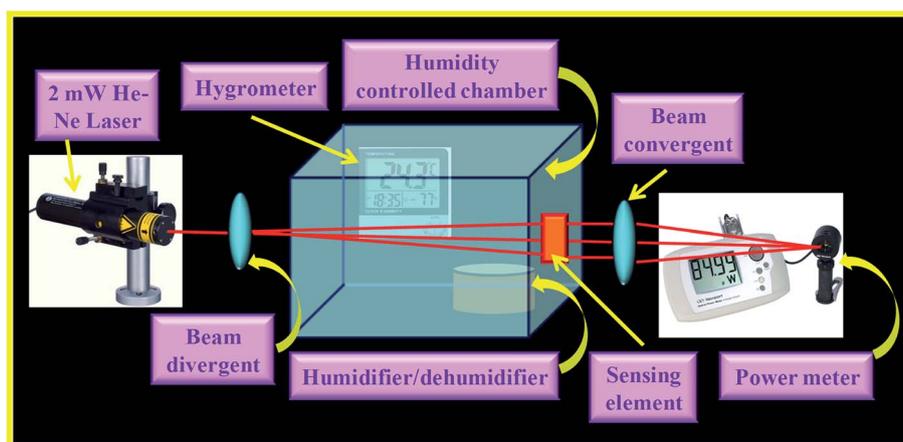
Fig. 1 Schematic of transmission based opto-electronic humidity sensing set-up.

surface area of the film. A beam condenser is used for converging the laser light beam to obtain the maximum intensity at a fixed point. An optical power meter (Newport 1916-R) is employed for detecting the modulated power of the transmitted beam by the sensing element. The detector part is kept perpendicular to the beam for obtaining the maximum output power and the whole experiment was performed on the Vibration Free Table (M-RS2000-48-8) at room temperature of 300 K.

Characterization techniques

The prepared film was investigated through a digital Refractometer (Anton Par Abbemat 550) in its original state at room temperature (300 K). The instrument is fast and non-destructive with a high accuracy of 0.000001. It is widely used for calibrating the official standards. TEM analysis of the material was carried out using Transmission Electron Microscope, JEOL JEM 200 CX. MnO_2–CoO precursor in diluted form was loaded over carbon coated copper grid with mesh size 200 at the scale of 50 nm. The morphological study of the film has been carried out at various scales and resolutions using Scanning Electron Microscope, JEOL JSM 840 A. The structural information of the film was studied by X-ray diffractometer X'Pert Pro recording system (PANalytical, Netherlands) using Cu K$_\alpha$ ($\lambda = 1.5406$ Å) radiation. The instrument was operated at 45 kV, 40 mA with scanning parameters of $0°$ to $70°$; typical 2θ step size: $0.008°$. Optical characterizations were done by obtaining Fluorescence, Photoluminescence and UV-Vis absorption spectrum. The Fluorescence and Photoluminescence spectrum of dilute precursor were obtained using Perkin-Elmer LS55 Luminescence spectrophotometer operated with a xenon discharge lamp (20 kW power) as the excitation source at room temperature in the visible range of the electromagnetic spectrum. UV-Vis absorption spectrum of the film was recorded in the wavelength regime of 190–1100 nm using UV-Vis Spectrophotometer (Evolution 201) with Hg lamp as the excitation source.

Results and discussion

Refractometer analysis

For the investigation of the refractive index of the film, the film was kept on the prism of the digital refractometer (Anton Par Abbemat 550) at room temperature and the piston of the instrument was pressed. Then screen showed the refractive index of the material as 1.445930.

Scanning electron microscopy (SEM)

The SEM images of the film at 10 μm, 5 μm and 1 μm are shown in Fig. 2(a–c) respectively. Surface morphology of the MnO_2–CoO thin films exhibits highly porous nature. The dimension of these pores is of micron order (as depicted in Fig. 2(c)); hence the film is macroporous in nature. This porosity enhances the surface area of the material and hence provides many dangling bonds suitable for adsorption/desorption of water molecule. These active centres serve as humidity adsorption sites and the sensitivity of the sensor depends on the availability of these dangling bonds.

Transmission electron microscopy (TEM)

Fig. 3 shows the TEM-SAED image of nanostructured MnO_2–CoO dilute precursor solution. Fig. 4(a) shows the SAED pattern of the material at 10 nm^{-1} scale. Here the concentric rings confirm the polycrystalline structure of nanocomposite. The indexing has been done for the observed rings of MnO_2 (tetragonal) and CoO (simple cubic) separately. Fig. 3(b) corresponds to the TEM image at 50 nm scale. It can be observed from the figure that there is uniform distribution of spherical particles of nano dimension. The minimum grain diameter as obtained from the micrograph is ~ 5.7 nm which is not yet reported in open literature.

X-ray diffraction (XRD)

Fig. 4(a) shows the XRD pattern of the film of nanostructured composite of MnO_2–CoO annealed at 650 °C. The asterisk (*)
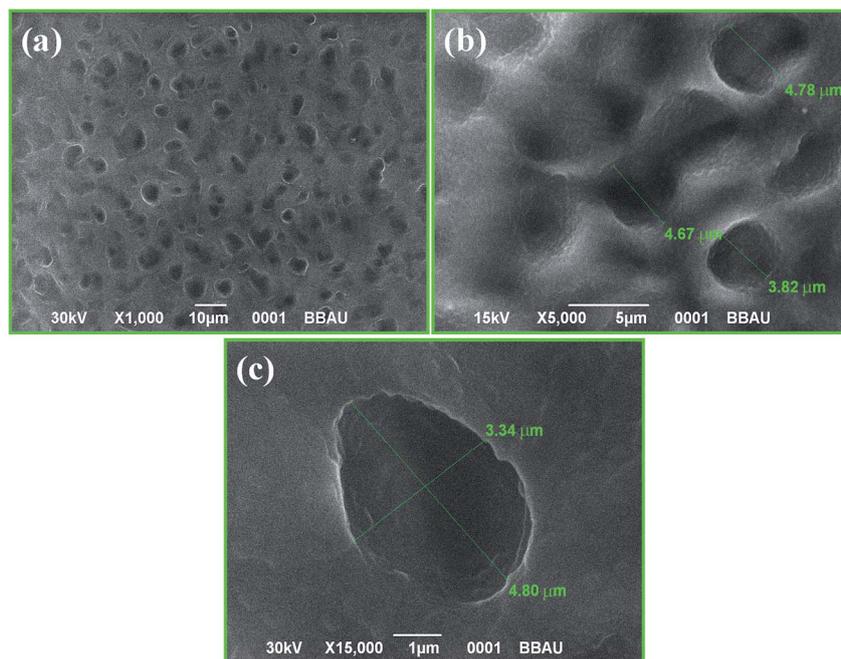
Fig. 2 SEM micrographs of nanostructured MnO_2–CoO thin film at (a) 10 μm, (b) 5 μm and (c) 1 μm, showing the porous nature and hence enhanced surface area and availability of more active sites suitable for adsorption/desorption of moisture.

peaks denote the MnO_2 crystals whereas hatch (#) peaks represent CoO crystals. The diffraction pattern shows good agreement with the diffraction data from JCPDS 240735 and 750 419 for MnO_2 crystals and CoO crystals respectively. The minimum crystallite size of the material was estimated as 4 nm using Debye–Scherrer Formula from (110) peak which is the least value of crystallite size reported in open literature. The crystallite size plays an important parameter in sensing as it increases the aspect ratio and hence provides more active centres for the adsorption/desorption of water molecules.

Fluorescence spectroscopy

Fluorescence spectroscopy is a contactless, non-destructive technique to probe the electronic structure of materials. Here,

the fluorescence spectrum is obtained in the wavelength regime of 400–750 nm. The spectrum is shown in Fig. 4(b) where the peak in the lower wavelength region shows the blue shifting with respect to that of the reported literature of the constituent materials[31,32] and hence confirms the low dimensionality of the nanostructured composite of MnO_2–CoO.

Photoluminescence spectroscopy

The PL spectrum of the dilute nanostructured MnO_2–CoO precursor was obtained at room temperature in the wavelength range of 350–750 nm. The spectrum is shown in Fig. 5(a). The intensity and spectral content of the emitted photoluminescence is a direct measure of numerous important material properties, as well as band gap determination,
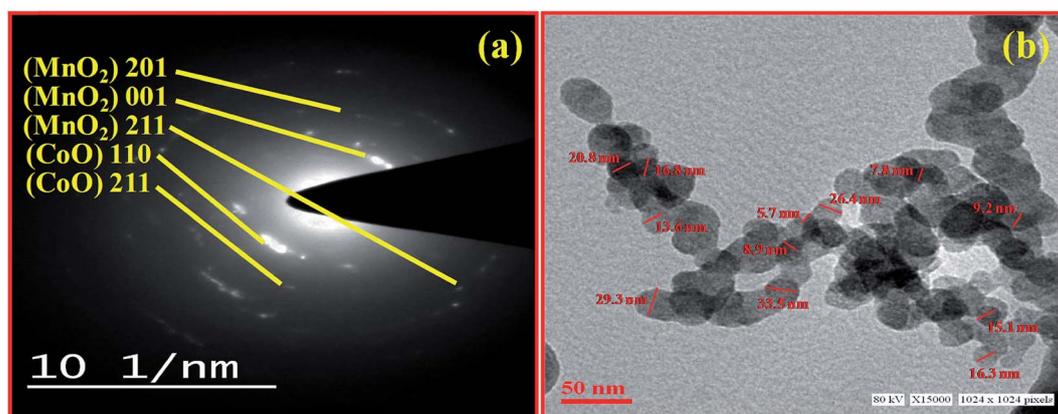

Fig. 3 Images showing (a) SAED pattern of the material where the concentric rings show the polycrystalline nature of MnO_2–CoO nanocomposite and (b) TEM image at 50 nm scale showing all the particles of nano dimension with minimum grain diameter of ∼5.7 nm.
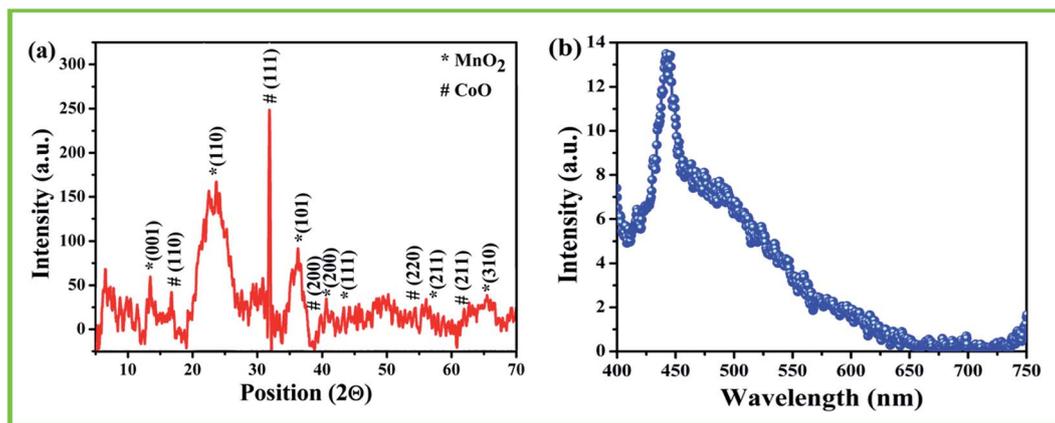
Fig. 4 Curves showing (a) XRD pattern of nanostructured MnO_2–CoO composite from which minimum crystallite size was estimated as 4 nm and (b) fluorescence spectrum of dilute MnO_2–CoO precursor in the visible regime of the electromagnetic spectrum where the blue shifted peak confirms its low dimension.

dirtiness levels, imperfection detection and recombination mechanisms. The shifting of the emission peak may be due to the non-uniform size of the particles (as confirmed from TEM) in the precursor sol.[33] The emission peaks at 380 nm and 400 nm corresponds to the violet emission, which may provide a new scope in the field of luminescent display materials.

UV-visible (UV-Vis) absorption analysis

The optical absorbance spectrum of the MnO_2–CoO thin film deposited on the flat borosilicate substrate was recorded in the wavelength range 190–1100 nm and is shown in Fig. 5(b). It is observed from data that film exhibits absorption in the ultra-violet range of the electromagnetic spectrum. Tauc curve (inset of Fig. 5(b)) was plotted to show the variation of the square of the optical absorption coefficient (α^2) with photon energy $h\nu$ from the absorption data. The optical energy band-gap E_g of the film can be estimated from the eqn (2):

$$E_g = h\nu - (\alpha h\nu)^{1/n}\ldots \quad (2)$$

where 'h' is Planck's constant, 'ν' is the transition frequency and the exponent 'n' characterizes the nature of band transition ($n = 1/2$ and 3/2, 2 and 3 corresponds to direct allowed and directly forbidden, indirect allowed and indirect forbidden transitions, respectively). Here the transition being the directly allowed type, therefore n is taken as 1/2 in the above equation. The optical energy band-gap E_g was obtained by extrapolating the straight line portion of Tauc curve to $\alpha = 0$. The estimated band-gap of the thin film was found to be 3.849 eV, which is quite high and hence it can also be used in various optical devices.

Humidity sensing

The optical humidity sensing characteristics for MnO_2–CoO thin film annealed at 650 °C has been investigated and plotted in Fig. 6(a). The curve shows an almost linear decrement in transmitted power with a corresponding increase in % RH in all the lower (10–30% RH), intermediate (30–70% RH) and higher regions of % RH (70–90% RH), maintaining a constant slope in the entire range of % RH. In our case, sensitivity is the most
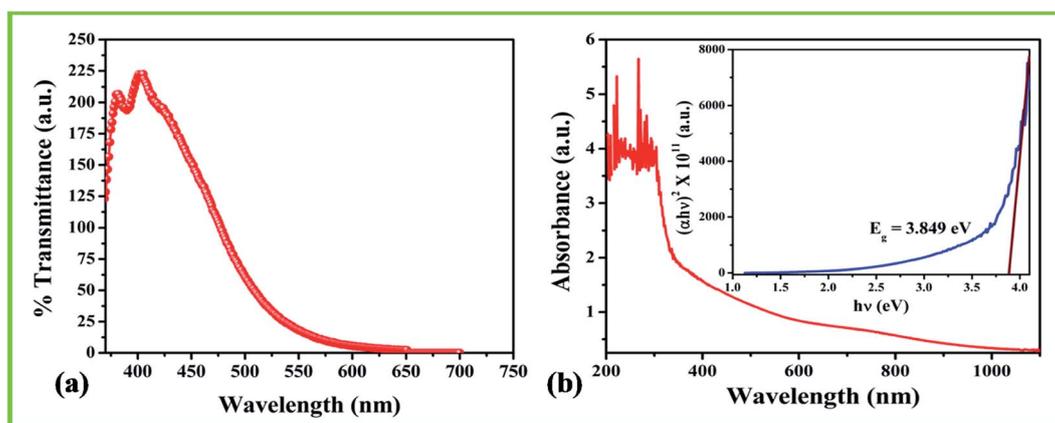

Fig. 5 Curves depicting at room temperature (a) photoluminescence spectrum in the wavelength regime of 350–750 nm where the peaks correspond to violet emission (b) absorption spectrum of thin film and inset display the Tauc plot for optical energy band-gap calculation showing the band-gap of 3.849 eV.
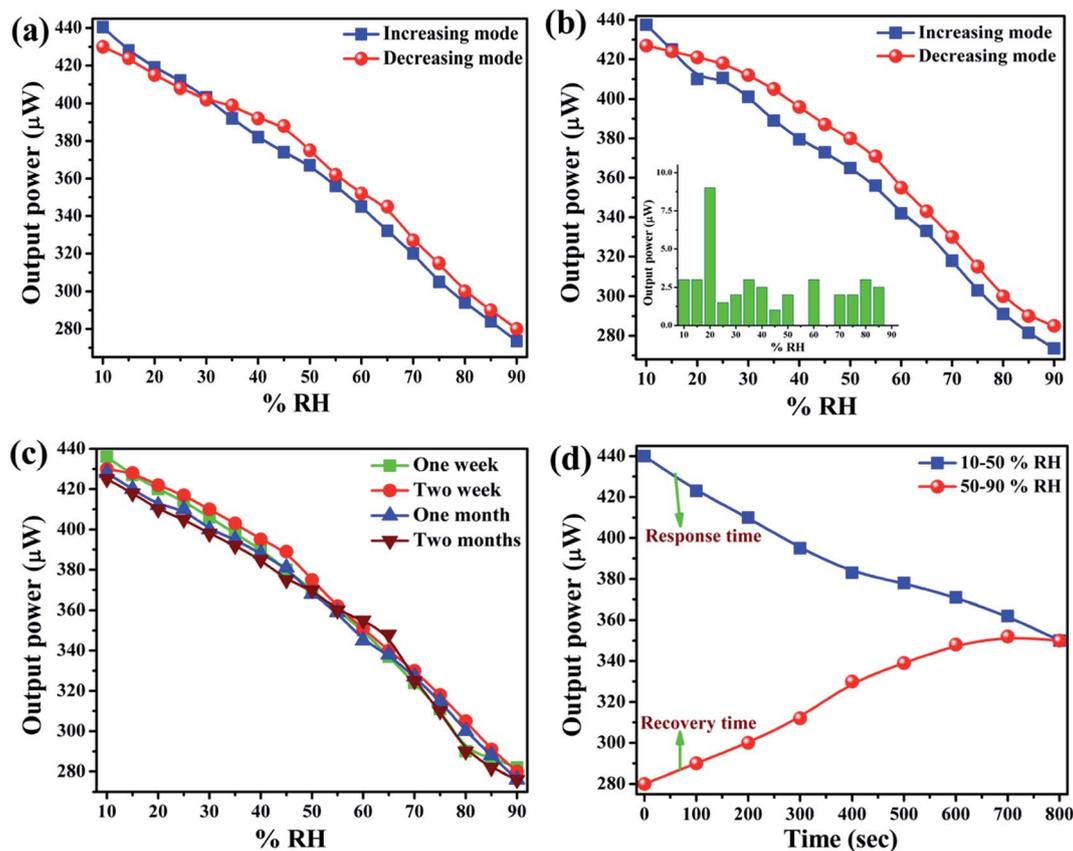
Fig. 6 Variation of transmitted power with % RH for nanostructured MnO_2–CoO thin film to investigate the [a] sensing response (sensitivity observed was 2.225 μW/% RH) [b] reproducibility characteristics (~89% reproducible with 1.969 μW/% RH in this case) where inset figure displays the error bars [c] aging effect (after one week, two weeks, one month and three months); and [d] response (47 s) and recovery (59 s) times.

concerned parameter, calculated by taking the slope of the sensing response curve. Also, the sensitivity is defined as the ratio of the change in output signal to that of input signal, as shown by eqn (3):

$$\text{Sensitivity} = \Delta I_t/\Delta\% \text{ RH μW/\% RH} \ldots \quad (3)$$

where ΔI_t is the change in transmitted power of laser light obtained at the detector and $\Delta\%$ RH is the relative change in % RH, measured from hygrometer. So, sensitivity has been calculated by taking the ratio of the difference in the initial and final readings of transmitted power to the corresponding difference in % RH. The sensitivity in the range 10–30% RH is 2.85 μW/% RH, 30–70% RH is 1.825 μW/% RH and 70–90% RH is 2 μW/% RH. The average sensitivity of the sensing element is taken as the average of all the values and is found ~2.225 μW/% RH as calculated from the blue-lined curve of Fig. 6(a). The red line in the curve of Fig. 6(a) shows the hysteresis while dehumidifying the environment inside the chamber. The average

sensitivity, in this case, is found as ~1.875 μW/% RH showing 15.73% hysteresis.

Reproducibility is another most concerned parameter for an efficient sensor. It is the distribution of output when measurements are taken under a similar environmental state of affairs as earlier.[34] Here the experiment for observing the reproducibility of sensor was performed and plotted in Fig. 6(b). The inset displays the error bars of the experiment. From the error bars, it can be observed that at 20% RH, there is maximum error whereas it is minimum at 55 and 65% RH. The sensitivity observed over the entire range of % RH, while observing the reproducibility, was 1.969 μW/% RH and results were found ~89% reproducible. This high reproducibility depicts the quite stable nature of the sensing element.

Ageing effect is also an important sensor parameter. It is the distribution of sensor outputs when performing consecutive readings under similar conditions after a long time. The consecutive measurements were taken after one week, two weeks, one month and two months showing as green, red, blue

Table 1 Sensing parameters for nanostructured MnO_2–CoO thin film based sensor

Sensor parameters	Average sensitivity	Hysteresis	Reproducibility	Response time	Recovery time	Aging effect
Values	2.225 μW/% RH	15.73%	~89%	47 s	59 s	Insignificant

Table 2 A brief literature review showing the humidity sensing capability of recently reported materials

S. no.	Material	Sensitivity	Ref
1	PMMA microfiber loop resonator (PMLR) coated with ZnO	0.1746 dBm/% RH	36
2	Graphene oxide/PVA	0.193 dB/% RH	37
3	$Cu(NO_3)_2 \cdot (AAm)_4 \cdot 2H_2O$	0.838 µW/% RH	18
4	Zinc oxide	0.88 µW/% RH	38
5	$Zn(NO_3)_2 \cdot (AAm)_4 \cdot 2H_2O$	1.831 µW/% RH	39
6	Cobalt titanate	1.84 µW/% RH	26
7	$MgTiO_2$	1.86 µW/% RH	34
8	Y_2O_3–ZrO_2	1.937 µW/% RH	27
9	$Sc(CH_2\text{=}CH\text{–}COO)_3$	2.1 µW/% RH	40
10	MnO_2–CoO	2.225 µW/% RH	Present work

and brown coloured curves respectively in Fig. 6(c). The almost perfect overlapping among the curves indicates that nanostructured MnO_2–CoO is a quite stable material having insignificant effect of ageing and the sensor is quite stable in the entire range of % RH.

Response and recovery times were also measured for the reported sensor. Response time is the time requisite to attain 10% of the final sensor output following stepwise ramping of % RH and recovery time is the time taken by the sensor signal to come back to its original value after a step concentration variation from a definite value to zero.[35] Here both the response and recovery times were calculated from Fig. 6(d) and it was observed that for sensing film, the response time was 47 s and the recovery time was 59 s. All the sensor parameters have been shown in Table 1.

Sensing mechanism

It may be noted here that the film shows encouraging sensitivity due to rapid adsorption and desorption rate. A brief literature review has been shown in Table 2. Nanostructured MnO_2–CoO gel having high refractive index 1.448829, has a greater angle of transmittance. The laser light intensity after being transmitted from the film was collected on a photodetector through a lens combination. Besides the beautiful spherical shaped clusters

and the flakes formation with enhanced surface morphology; wide optical energy band-gap is also an important factor responsible for high sensitivity of the sensing element. The low dimension of the material is also a very important factor responsible for good sensing property. As the grain size decreases, the aspect (surface to volume) ratio increases. By increasing aspect ratio more active sites for adsorption/ desorption can be generated. It was observed that as the humidity inside the chamber increases, the transmitted power observed at the detector decreases. This decrease in output power with the corresponding increase in % RH is the responsible characteristic for its application as an opto-electronic humidity sensor.

The change in the transmitted power with respect to variation of % RH can be explained on the basis of adsorption and desorption mechanism of the water molecule in the capillaries formed on the surface of nanostructured bimetallic oxide thin film. The sensing mechanism, dependent on the surface morphology is based on the chemisorption and physisorption of a water molecule. In the beginning, the nanostructured bimetallic oxide thin film was free from water molecules with only dehydrated air in its pores. When humidity was created inside the chamber using a humidifier, then at the low humid environment, adsorption of water vapour takes place rapidly on
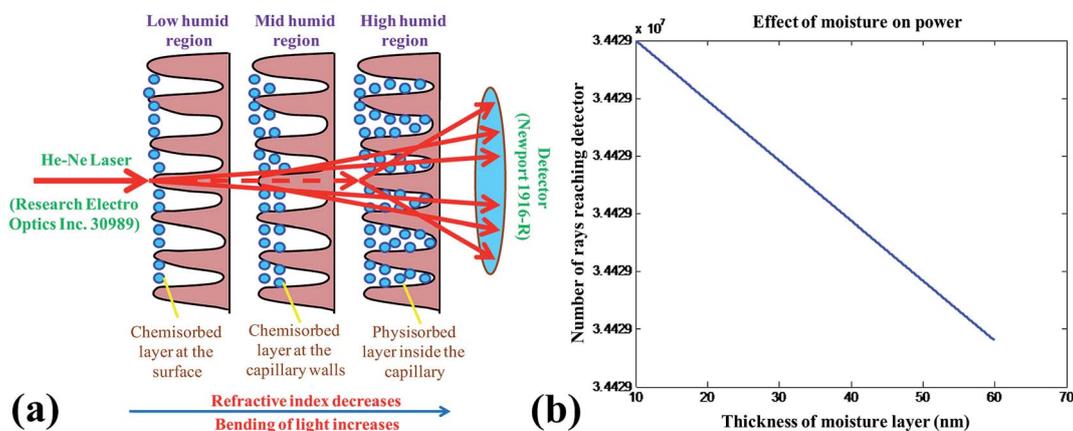

Fig. 7 (a) Ray diagram of sensing mechanism showing the decrease in output power with exposure of % RH showing (i) surface chemisorption at lower humidity (10–30% RH), (ii) chemisorption on capillary walls at intermediate humidity (30–70% RH) and (iii) physisorption with full capillary condensation at higher humidity (70–90% RH) (b) Theoretical results confirming the experimental results.

the surface of the film. The metal oxide surface being highly electrovalent has sufficient electrostatic force to break one of the O–H bonds of H_2O and form a strong chemical bond between M^+ (metal ion) and OH^- and forms the chemisorbed layer. With the increase in % RH inside the chamber, adsorption on the surface of the film increases and the refractive index of the material decreases and tends to the bending of transmitted laser light beam. In the mid humidity range (30–70% RH), adsorption of water vapour in the form of OH^- ion not only takes place on the surface but also on the walls of capillaries of the film. This leads to the increase in the thickness of moisture layer which tends to a lateral shift of the transmitted light from the sensing element. So the number of light rays reaching the detector gradually decreases and therefore less power is obtained at the output. In high humid region (70–90% RH), the condensation of water vapour takes place through the capillaries and forms a meniscus in the capillaries of the film in the form of a physisorbed layer. In this range, moisture layer acquires the maximum thickness and thus the lateral shift of transmitted light takes place to its maximum level. Hence the highest reduction in transmitted power is obtained, as most of the power could not reach the detector and is scattered in the surroundings.[41–43] The whole sensing mechanism has been explained by ray diagram in Fig. 7(a). The number of rays reaching the detector has been calculated on the above mentioned theoretical concept and the results well matched with the observed values as shown in Fig. 7(b).

Conclusions

Nanostructured MnO_2–CoO was successfully synthesized using metal carboxylates as precursors and thin films were fabricated via spin coating technique and annealed at 650 °C. TEM investigated the minimum grain diameter of ~5.7 nm and SAED confirmed the polycrystalline nature. The minimum crystallite size as obtained from XRD was ~4 nm. SEM micrographs showed the enhanced surface area of the film by the formation of pores on the surface of the film. The study of the photoluminescence showed the peak in the violet region. The Tauc plot obtained from the UV-Vis absorption spectrum estimated the optical energy band gap of 3.849 eV. The film was then employed efficaciously as opto-electronic humidity sensor and the average sensitivity was found as 2.225 μW/% RH along with the response and recovery times as 47 s and 59 s.

Conflicts of interest

There are no conflicts to declare.

Acknowledgements

References

1 G. Korotcenkov, J. Mater. Sci. Eng. B, 2007, 139, 1–23.

2 E. Kanazawa, G. Sakai, K. Shimanoe, Y. Kanmura, Y. Teraoka, N. Miura and N. Yamazoe, Sens. Actuators, B, 2001, 77, 72–77.

3 X. W. Xie, Y. Li, Z. Q. Liu, M. Haruta and W. J. Shen, Nature, 2009, 458, 746–749.

4 C. S. Pan, D. S. Zhang, L. Y. Shi and J. H. Fang, Eur. J. Inorg. Chem., 2008, 15, 2429–2436.

5 S. L. Brock, N. Duan, Z. R. Tian, O. Giraldo, H. Zhou and S. L. Suib, Chem. Mater., 1998, 10, 2619–2628.

6 Y. Li, X. Y. Yang, Y. Feng, Z. Y. Yuan and B. L. Su, Synthesis, Characterizations, Properties and Applications, Crit. Rev. Solid State Mater. Sci., 1998, 37(1), 1–74.

7 J. Dakin and B. Culshaw, Optical Fiber Sensors: Principles and Components, Artech House, 1st edn, Boston, 1988.

8 J. F. Liu, X. Wang, Q. Peng and Y. D. Li, Adv. Mater., 2005, 17, 764–767.

9 X. Zhang, G. Wang, W. Zhang, N. Hu, H. Wu and B. Fang, J. Phys. Chem. C, 2008, 112, 8856–8862.

10 G. I. Dzhardimalieva and A. D. Pomogailo, Macromolecular metal carboxylates as precursors of metallopolymer nanocomposites, in Chapter in Book: Nanocomposites: In Situ Synthesis of Polymer-Embedded Nanostrutures, ed. L. Nicolais and G. Carotenuto, John Wiley & Sons Inc., Hoboken, New Jersey, 2014, pp. 97–114.

11 D. Pomogailo and G. I. Dzhardimalieva, Nanostructured Materials Preparation via Condensation Ways, Springer, 2014, p. 460.

12 M. Lawecka, A. Slawska-Wanievska, K. Racka, M. Leonowicz, G. I. Dzhardimalieva, A. S. Rozenberg and A. D. Pomogailo, J. Alloys Compd., 2004, 369, 244.

13 X. M. Liu and S. Y. Fu, J. Magn. Magn. Mater., 2007, 308(1), 61–64.

14 X. M. Liu, S. Y. Fu, H. M. Xiaoa and C. J. Huang, Phys. B, 2005, 370, 14.

15 H. M. Xiao, X. M. Liu and S. Y. Fu, Compos. Sci. Technol., 2006, 66, 2003–2008.

16 S. Sikarwar and B. C. Yadav, Sens. Actuators, A, 2015, 233, 54–70.

17 Y. Zhou, H. Wang, M. Sheng, Q. Zhang, Z. Zhao, Y. Lin, H. Liu and G. R. Patzke, Sens. Actuators, B, 2013, 188, 1312–1318.

18 P. Chaudhary, S. Sikarwar, B. C. Yadav, G. I. Dzhardimalieva, N. D. Golubeva and I. E. Uflyand, Sens. Actuators, A, 2017, 263, 415–422.

19 J. Ascorbe, J. M. Corres, I. R. Matias and F. J. Arregui, Sens. Actuators, B, 2016, 233, 7–16.

20 B. V. Golovkin and G. V. Bazuev, Russ. J. Gen. Chem., 2010, 80(2), 213–218.

21 C. Li, J. Balamurugan, T. D. Thanh, N. H. Kim and J. H. Lee, J. Mater. Chem. A, 2017, 5, 397–408.

22 W. Huang, H. Zhong, D. Li, P. Tang and Y. Feng, *Electrochim. Acta*, 2015, **173**, 575–580.

23 T. Kato, Y. Tanaka, T. Hirata, S. Kumamoto and K. Miyazaki, *J. Mater. Sci. Lett.*, 1997, **16**, 1771–1773.

24 K. Miyazaki, M. Hieda and T. Kato, *Ind. Eng. Chem. Res.*, 1997, **36**, 88–91.

25 M. Z. Yang, C. L. Dai, P. J. Shih and Y. C. Chen, *Microelectron. Eng.*, 2011, **88**, 1742–1744.

26 B. C. Yadav, R. C. Yadav, S. Singh, P. K. Dwivedi, H. Ryu and S. Kang, *Opt. Laser Technol.*, 2013, **490**, 68–74.

27 S. Sikarwar, B. C. Yadav, S. Singh, G. I. Dzhardimalieva, S. I. Pomogailo, N. D. Golubeva and A. D. Pomogailo, *Sens. Actuators, B*, 2016, **232**, 283–291.

28 L. E. Scriven, *Mater. Res. Soc. Symp. Proc.*, 1988, **121**, 717–729.

29 T. K. Pathak, J. K. Rajput, V. Kumar, L. P. Purohit, H. C. Swart and R. E. Kroon, *J. Colloid Interface Sci.*, 2017, **487**, 378–387.

30 D. A. H. Hanaor, G. Triani and C. C. Sorrell, *Surf. Coat. Technol.*, 2011, **205**(12), 3658–3664.

31 S. Prasad and A. Patra, *Green Process. Synth.*, 2017, **6**(6), 549–554.

32 B. K. Pandey, A. K. Shahi and R. Gopal, *Appl. Surf. Sci.*, 2015, **347**, 461–470.

33 D. P. Singh, S. Pandey, S. K. Gupta, R. Manohar, A. Daoudi, A. H. Sahraoui, C. Phadnis and S. Mahamuni, *J. Lumin.*, 2016, **173**, 250–256.

34 B. C. Yadav, R. C. Yadav and P. K. Dwivedi, *Sens. Actuators, B*, 2010, **148**, 413–419.

35 S. Kozhukharov, Z. Nenova, T. Nenov, N. Nedev and M. Machkova, *Sens. Actuators, B*, 2015, **210**, 676–684.

36 N. Irawati, T. N. R. Abdullah, H. A. Rahman, H. Ahmad and S. W. Harun, *Sens. Actuators, A*, 2017, **260**, 112–116.

37 Y. Wang and C. Shen, *Opt. Commun.*, 2016, **372**, 229–234.

38 B. C. Yadav, R. C. Yadav and G. C. Dubey, *Opt. Appl.*, 2009, **39**(3), 617–627.

39 B. C. Yadav, S. Sikarwar, R. Yadav, P. Chaudhary, G. I. Dzhardimalieva and N. D. Golubeva, *J. Mater. Sci.: Mater. Electron.*, 2018, 1–8.

40 S. Sikarwar, A. Kumar, B. C. Yadav, G. I. Dzhardimalieva and N. D. Golubeva, *IEEE Sens. J.*, 2018.

41 F. Xu, L. Zhang, X. Yin and L. Tong, Polymer single-Nanowire Optical Sensors, *Nano Lett.*, 2008, **8**, 2757–2761.

42 B. C. Yadav, K. S. Chauhan, S. Singh, R. K. Sonker, S. Sikarwar and R. Kumar, *J. Mater. Sci.: Mater. Electron.*, 2017, **28**, 5270–5280.

43 Z. Nenova, S. Kozhukharov, T. Nenov, N. Nedev and M. Machkova, *Sens. Actuators, B*, 2016, **224**, 143–152.